Hole-$s_\pm$ State Induced by Coexisting Ferro- and Aniferromagnetic and Aniferro-orbital Fluctuations in Iron Pnictides

Jun Ishizuka[1], Takemi Yamada[1], Yuki Yanagi[2], Yoshiaki Ōno[1]

1. Department of Physics, Niigata University, Ikarashi, Niigata 950-2181, Japan
2. Department of Physics, Faculty of Science and Technology, Tokyo University of Science, Noda 278-8510, Japan

The five-orbital Hubbard model for iron-based superconductors is investigated by using the dynamical mean-field theory combined with the Eliashberg equation to clarify the local correlation effects on the electronic states and the superconductivity. In the specific case where the antiferromagnetic (AMF) and the antiferro-orbital (AFO) fluctuations are comparably enhanced, the orbital dependence of the vertex function becomes significantly large while that of the self-energy is small, in contrast to the AFM fluctuation-dominated case where the vertex function (the self-energy) shows small (large) orbital dependence. The orbital-dependent vertex function together with the nesting between the inner and outer hole Fermi surfaces results in the enhancement of the inter-orbital ferromagnetic (FM) fluctuation in addition to the AFM and AFO fluctuations. In this case, the hole-$s_\pm$-wave pairing with the sign change of the two hole Fermi surfaces is mediated by the coexisting three fluctuations as expected to be observed in a specific compound LiFeAs.

KEYWORDS: dynamical mean-field theory, iron-based superconductor, magnetic fluctuation, orbital fluctuation, 5-orbital Hubbard model

1. Introduction

Since the discovery of superconductivity with high transition temperature in $LaFeAsO_{1-x}F_x$,[1)] numerous investigations have been carried out for the iron-based superconductors categorized into four families: the 1111 system such as LaFeAsO, the 122 system such as $BaFe_2As_2$, the 111 system such as LiFeAs and the 11 system such as FeSe.[2,3)] Most of the 1111 and the 122 systems show the stripe-type antiferromagnetic (AFM) transition at T_N and the tetragonal-orthorhombic structural transition at T_s just above T_N. Correspondingly, the AFM fluctuation diverges towards T_N and the ferro-orbital (FO) fluctuation responsible for the softening of the elastic constant C_{66}[4–6)] diverges towards T_s. Therefore, the AFM and the FO fluctuations have been discussed as key ingredients for the pairing mechanisms.

Theoretically, the AFM fluctuation for $\boldsymbol{q} \sim (\pi, 0)$ corresponding to the nesting wave vector between electron and hole Fermi surfaces (FSs) was found to be enhanced by the onsite Coulomb interaction between Fe d electrons and mediates the $s_\pm$-wave pairing where the gap function changes its sign between the electron and the hole FSs.[7,8)] On the other hand, the FO fluctuation was found to be enhanced by the electron-phonon interaction[9)] and/or the mode-coupling,[10,11)] where the antiferro-orbital (AFO) fluctuation for $\boldsymbol{q} \sim (\pi, 0)$ was also enhanced due to the nesting as similar to the AFM fluctuation.[9–13)] When the AFO fluctuation overcomes the AFM fluctuation, the s_{++}-wave pairing without the sign change of the gap function was found to be realized with the help of the FO fluctuation.[9–13)] At the moment it is not clear which fluctuation is dominant, since the AFO fluctuation has not been explicitly observed in experiments so far.[14)] In either case, the AFM and the AFO fluctuations for the same $\boldsymbol{q}$ compete with each other resulting in suppression of the superconducting transition temperature T_c as compared to the case with either fluctuation alone.

Recently, we have proposed another mechanism of the FO fluctuation enhancement without enhancing the AFO fluctuation[15)] by taking into account of the orbital polarization interaction which is derived from the significant orbital dependence of the intersite d-p Coulomb integrals and is considered to be crucial in explaining the recent observation of strong coupling of Fe and As orbital polarizations observed in the electron diffraction experiment.[16)] In this mechanism, the FO fluctuation mediates the s-wave pairing within each of the electron and the hole FSs almost independently of each other, while the AFM fluctuation causes the pair scattering between the electron and hole FSs resulting in the $s_\pm$-wave pairing. Then, the AFM and FO fluctuations cooperatively enhance T_c without any competition by virtue of the $\boldsymbol{q}$-space segregation of the two fluctuations. By considering the suitable intersite d-p Coulomb integrals which are large for the 11 system FeSe relative to for the 1111 and the 122 systems,[17)] we can reproduce the phase diagram of FeSe under the pressure P where T_s monotonically decreases with increasing P while T_N which is absent for the ambient pressure becomes finite and increases with increasing P,[18)] together with the phase diagrams of the 1111 and the 122 systems where the both T_s and $T_N (< T_s)$ decrease with increasing the carrier doping.

In contrast to the systems mentioned above, the 111 system LiFeAs shows the superconductivity without any structural transitions and magnetic orders.[19)] The absence of the structural transition accompanied by the elastic softening seems to be consistent with the above mentioned FO fluctuation mechanism since the As-p orbital weights on the FSs for LiFeAs obtained from the first-principles band calculations are certainly smaller than those for the other systems exhibiting the structural transitions. Although the magnetic order is absent, the incommensurate magnetic fluctuation nearly to the AFM one was observed by the inelastic neutron scattering experiments,[20,21)] which is well accounted for by the nesting between the hole and the electron FSs observed by the angle-resolved photoemission spectroscopy (ARPES) experiment.[22)] In addition, the FM fluctuation was also observed by the μSR measurement.[23)] The recent NMR experiment revealed the FM fluctuation also for the 122 systems over a wide

doping range.[24] Therefore, the existence of the FM fluctuation may be a common feature of the iron-based superconductors as predicted from the first-principles band calculation.[25]

As a possible pairing symmetry of LiFeAs, the spin-triplet p-wave state with the nodes of the gap function on the hole FS mediated by the FM fluctuation was proposed on the basis of the effective three-orbital Hubbard model, where the FM fluctuation is largely enhanced relative to the AFM one because of the bad nesting between the hole and the electron FSs together with the flatness of the hole band top which yields the large density of states near the Fermi level responsible for the Stoner enhancement of the magnetic susceptibility.[26] A more realistic five-orbital Hubbard model for LiFeAs was investigated by using the dynamical mean-field theory (DMFT) which includes the local correlation effects sufficiently and was found to show the orbital antiphase $s_{\pm}$-wave pairing mediated by the AFM fluctuation observed to be much larger than the FM one, in which the gap function changes its sign between the hole FSs and has nodes on the electron FSs due to the strong repulsion between the $d_{zx(yz)}$ and d_{xy} orbitals.[27] In addition, several authors have proposed the hole-$s_{\pm}$-wave pairing with the sign change between the hole FSs without any nodes mediated by the AFM fluctuations with $\boldsymbol{q} \sim (\pi, \pi)$ in addition to $\boldsymbol{q} \sim (\pi, 0)$[28] and by the AFO fluctuation which is enhanced comparably to the AFM one by taking into account of the electron-phonon interaction or the mode-coupling effect.[29]

In our previous work,[30] the five-orbital Hubbard model for iron-based superconductors was studied by using the DMFT combined with the Eliashberg equation in which the effective pairing interaction mediated by the spin, charge and orbital fluctuations are obtained from the corresponding DMFT susceptibilities to discuss the superconductivity in the strong correlation regime where the magnetic and/or the orbital orders take place. It was found that the $s_{\pm}$-wave pairing is realized for $U > U'$ where the magnetic fluctuation dominates over the orbital one, while the s_{++}-wave pairing is realized for $U < U'$ where the orbital fluctuation dominates over the magnetic one. All of the critical interactions towards the magnetic, orbital and superconducting instabilities are suppressed as compared with the results from the random phase approximation (RPA), but the s_{++}-wave phase is largely expanded as compared with the RPA result in contrast to the s_{+-}-wave phase which is reduced due to the different renormalization effects between the spin and the charge-orbital vertices.

In this paper, we investigate the five-orbital Hubbard model for iron-based superconductors by using the DMFT, especially focusing on the specific case with $U \sim U'$ where the AFM and the AFO fluctuations are comparably enhanced. Then, we discuss the pairing symmetry in the case with the cooperating AFM and AFO fluctuations as expected to be realized in LiFeAs.[29] Although the case with $U \sim U'$ is not realistic, the AFO fluctuation is known to be largely enhanced by the electron-phonon interaction and possibly dominates over the AFM one even for the realistic case with $U > U'$.[31,32] In fact, a kink structure of the single-particle dispersion around the Γ point is observed experimentally in LiFeAs and is considered due to the effect of the strong electron-phonon coupling.[33] Thus, we expect that the present results with $U \sim U'$ are realized also for the realistic parameter with $U > U'$ by taking into account of the suitable electron-phonon interaction.

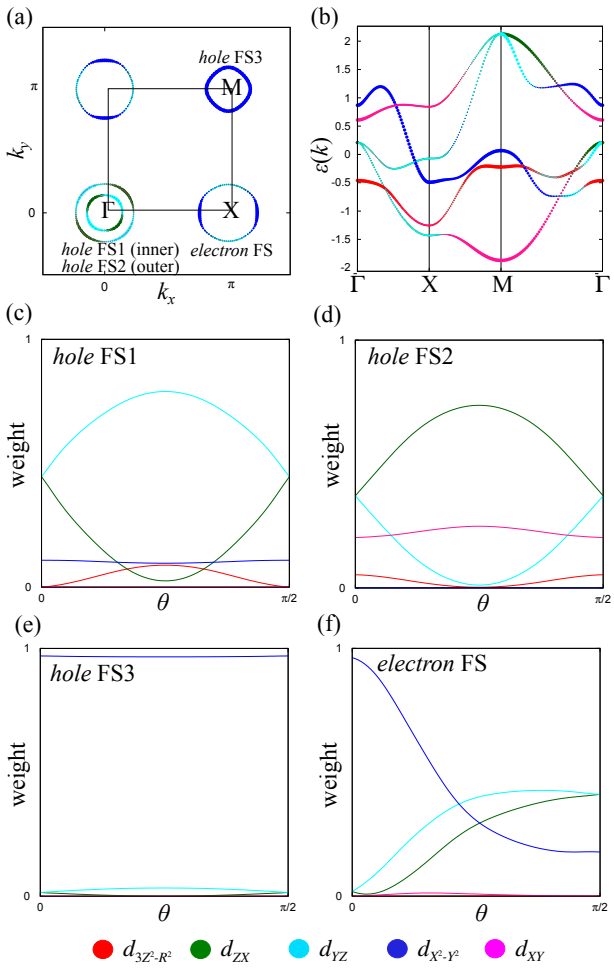

Fig. 1. (Color online) (a) The FSs of the five-orbital model (b) The dispersion of the band structure. (c)-(f) The weights of d orbitals on the FSs, where the horizontal axis is $\theta = \tan^{-1}(k_y/k_x)$. We set the Fe-3$d$ orbitals as follows: (1) $d_{3Z^2-R^2}$ (red), (2) d_{ZX} (green), (3) d_{YZ} (cyan), (4) $d_{X^2-Y^2}$ (blue) and (5) d_{XY} (pink).

2. Model and Formulation

The five-orbital Hubbard model for iron-pnictides is given by the following Hamiltonian,

$$H = H_0 + H_{\rm int}, \tag{1}$$

where the kinetic part $\hat{H}_0$ is determined so as to reproduce the first-principles band structure and its FSs for LaFeAsO[34] as shown in Fig. 1, where the weights of orbitals on the FSs are also plotted. In eq. (1), the Coulomb interaction part $H_{\rm int}$ includes the multi-orbital interaction on Fe sites: the intra- and inter-orbital direct terms U and U', the Hund's rule coupling J and the pair transfer J', and is explicitly given by

$$\begin{aligned} H_{\rm int} &= \frac{1}{2}U \sum_i \sum_\ell \sum_{\sigma\neq\bar{\sigma}} d^\dagger_{i\ell\sigma} d^\dagger_{i\ell\bar{\sigma}} d_{i\ell\bar{\sigma}} d_{i\ell\sigma} \\ &+ \frac{1}{2}U' \sum_i \sum_{\ell\neq\bar{\ell}} \sum_{\sigma,\sigma'} d^\dagger_{i\ell\sigma} d^\dagger_{i\bar{\ell}\sigma'} d_{i\bar{\ell}\sigma'} d_{i\ell\sigma} \\ &+ \frac{1}{2}J \sum_i \sum_{\ell\neq\bar{\ell}} \sum_{\sigma,\sigma'} d^\dagger_{i\ell\sigma} d^\dagger_{i\bar{\ell}\sigma'} d_{i\ell\sigma'} d_{i\bar{\ell}\sigma} \end{aligned}$$

$$+ \quad \frac{1}{2}J' \sum_i \sum_{\ell \neq \bar{\ell}} \sum_{\sigma \neq \bar{\sigma}} d^\dagger_{i\ell\sigma} d^\dagger_{i\ell\bar{\sigma}} d_{i\bar{\ell}\bar{\sigma}} d_{i\bar{\ell}\sigma}, \qquad (2)$$

where $d_{i\ell\sigma}$ is the annihilation operator for Fe-3d electrons with spin σ in the orbital ℓ at the site i. In the present paper, we set $d_{3Z^2-R^2}, d_{ZX}, d_{YZ}, d_{X^2-Y^2}$, and d_{XY} orbitals as 1,2,3,4 and 5, where x, y axes (X, Y axes) are along the nearest Fe-Fe (Fe-As) directions.

To solve the model eq. (1), we use the DMFT[35] in which the lattice model is mapped onto impurity Anderson model embedded in an effective medium that may be described by the frequency dependent effective action. In the actual calculations with the DMFT, we solve the effective five-orbital impurity Anderson model, where the Coulomb interaction at the impurity site is given by the same form as $\hat{H}_{\rm int}$ with a site i, and the kinetic energy responsible for the bare impurity Green's function $\hat{\mathcal{G}}$ in the 5×5 matrix representation is determined so as to satisfy the self-consistency condition as possible. We use the exact diagonalization (ED) method for a finite-size cluster as an impurity solver to obtain the local quantities such as the self-energy $\hat{\Sigma}$. To avoid CPU-time consuming calculation, we employ the clusters with the site number $N_s = 4$ within a restricted Hilbert space, as used in our previous paper;[30] where we approximate the clusters with those of $d_{3Z^2-R^2}$ and d_{XY} orbital by $N_s = 2$ since the two orbitals are far from the Fermi energy in contrast to the another three orbitals. We have confirmed that the results with $N_s = 4$ are qualitatively consistent with those with $N_s = 2$[36] and quantitatively improved especially for the intermediate interaction regime. Moreover, the studies by the slave-spin mean field,[37–39] the slave-boson mean field (Gutzwiller)[40] approximations, and also the DMFT with the continuous-time quantum Monte Carlo method (CT-QMC)[41] give a similar results over our approach. Then, we expect that the present calculation is sufficiently accurate at least up to the intermediate regime.

Within the DMFT, the spin (charge-orbital) susceptibility is given in the 25×25 matrix representation as

$$\hat{\chi}_{s(c)}(q) = \left[1 - (+)\hat{\chi}_0(q)\hat{\Gamma}_{s(c)}(i\omega_n)\right]^{-1} \hat{\chi}_0(q), \qquad (3)$$

with $\hat{\chi}_0(q) = -(T/N)\sum_k \hat{G}(k+q)\hat{G}(k)$, where $\hat{G}(k) = [(i\varepsilon_m + \mu) - \hat{H}_0(\boldsymbol{k}) - \hat{\Sigma}(i\varepsilon_m)]^{-1}$ is the lattice Green's function, $\hat{H}_0(\boldsymbol{k})$ is the kinetic part of the Hamiltonian with the wave vector $\boldsymbol{k}$, $\hat{\Sigma}(i\varepsilon_m)$ is the lattice self-energy, which coincides with the impurity self-energy obtained in impurity Anderson model, and $k = (\boldsymbol{k}, i\varepsilon_m)$, $q = (\boldsymbol{q}, i\omega_n)$. Here, $\varepsilon_m = (2m+1)\pi T$ and $\omega_n = 2n\pi T$ are fermionic and bosonic Matsubara frequencies. In eq. (3), $\hat{\Gamma}_{s(c)}(i\omega_n)$ is the local irreducible spin (charge-orbital) vertex function in which only the external frequency (ω_n) dependence is considered as a simplified approximation[30,42] and is explicitly given by

$$\hat{\Gamma}_{s(c)}(i\omega_n) = -(+)\left[\hat{\chi}^{-1}_{s(c)}(i\omega_n) - \hat{\chi}^{-1}_0(i\omega_n)\right], \qquad (4)$$

with $\hat{\chi}_0(i\omega_n) = -T\sum_{\varepsilon_m} \hat{G}(i\varepsilon_m + i\omega_n)\hat{G}(i\varepsilon_m)$, where $\hat{\chi}_{s(c)}(i\omega_n)$ is the local part of spin (charge-orbital) susceptibility. When the largest eigenvalue $\alpha_s(\boldsymbol{q})$ [$\alpha_c(\boldsymbol{q})$] of $(-)\hat{\chi}_0(q)\hat{\Gamma}_{s(c)}(i\omega_n)$ in eq. (3) for a wave vector $\boldsymbol{q}$ with $i\omega_n = 0$ reaches unity, the instability towards the magnetic (charge-orbital) order with the corresponding $\boldsymbol{q}$ takes place, and then $\alpha_s(\boldsymbol{q})$ [$\alpha_c(\boldsymbol{q})$] is called spin (charge-orbital) Stoner factor. After convergence of the DMFT self-consistent loop, the quantity $\hat{\chi}_{s(c)}(i\omega_n)$ in eq. (4) is obtained by means of continued fraction algorithm.[35]

The effective pairing interaction mediated by the spin and charge-orbital fluctuations is written by using the spin (charge-orbital) susceptibility in eq. (3) and the spin (charge-orbital) vertex in eq. (4), and is explicitly given for the spin-singlet state as

$$\hat{V}(q) = \frac{3}{2}\hat{\Gamma}_s(i\omega_n)\hat{\chi}_s(q)\hat{\Gamma}_s(i\omega_n) - \frac{1}{2}\hat{\Gamma}_c(i\omega_n)\hat{\chi}_c(q)\hat{\Gamma}_c(i\omega_n) + \frac{1}{2}\left(\hat{\Gamma}^{(0)}_s + \hat{\Gamma}^{(0)}_c\right) \qquad (5)$$

with the bare spin (charge-orbital) vertex: $[\hat{\Gamma}^{(0)}_{s(c)}]_{\ell\ell\ell\ell} = U(U)$, $[\hat{\Gamma}^{(0)}_{s(c)}]_{\ell\ell'\ell\ell'} = U'(-U'+2J)$, $[\hat{\Gamma}^{(0)}_{s(c)}]_{\ell\ell\ell'\ell'} = J(2U'-J)$ and $[\hat{\Gamma}^{(0)}_{s(c)}]_{\ell\ell'\ell'\ell} = J'(J')$, where $\ell' \neq \ell$ and the other matrix elements are 0. Substituting the effective pairing interaction in eq. (5) into the linearized Eliashberg equation:

$$\lambda\Delta_{ll'}(k) = -\frac{T}{N}\sum_{k'}\sum_{l_1 l_2 l_3 l_4} V_{ll_1,l_2l'}(k-k') \times G_{l_3 l_1}(-k')\Delta_{l_3 l_4}(k')G_{l_4 l_2}(k'), \qquad (6)$$

we obtain the gap function $\Delta_{ll'}(k)$ with the eigenvalue λ which becomes unity at the superconducting transition temperature $T = T_c$. To solve eq. (6), we neglect the frequency dependence of the vertex $\hat{\Gamma}_{s(c)}(i\omega_n) \approx \hat{\Gamma}_{s(c)}(i\omega_n = 0)$ for simplicity of the numerical calculations but the effect of the frequency dependence will be discussed later. We note that, eq. (6) yields the RPA result of $\Delta_{ll'}(k)$ when we replace $\hat{\Gamma}_{s(c)}$ with $\hat{\Gamma}^{(0)}_s$ and neglect $\hat{\Sigma}$, and then, is a straightforward extension of the RPA to include the vertex and the self-energy corrections within the DMFT.[30]

All calculations are performed for the electron number $n = 6.0$ corresponding to the non-doped case at $T = 0.02$eV except for the ED calculation in the impurity Anderson model where we calculate the self-energy at $T = 0$ as the explicit T-dependence is expected to be small at low temperature $T = 0.02$eV in the intermediate correlation regime with $Z \gtrsim 0.5$. We use 32×32 $\boldsymbol{k}$-point meshes and 1024 Matsubara frequencies in the numerical calculations with the fast Fourier transformation. Here and hereafter, we measure the energy in units of eV.

3. Numerical Results

In the previous paper,[30] we investigated the model eq. (1) by using the DMFT combined with the Eliashberg equation as mentioned in Sec. 2, and found that the $s_\pm$-wave pairing is realized for $U > U'$ where the magnetic fluctuation dominates over the orbital one, while the s_{++}-wave pairing is realized for $U < U'$ where the orbital fluctuation dominates over the magnetic one. In the present paper, we focus on the typical parameter with $U \sim U'$ and vary U with keeping $U = U' - 0.2$ and $J = J' = 0.15$ to simulate the specific case where the magnetic and the orbital fluctuations are comparably enhanced in the intermediate region of $U > U'$ and $U < U'$.

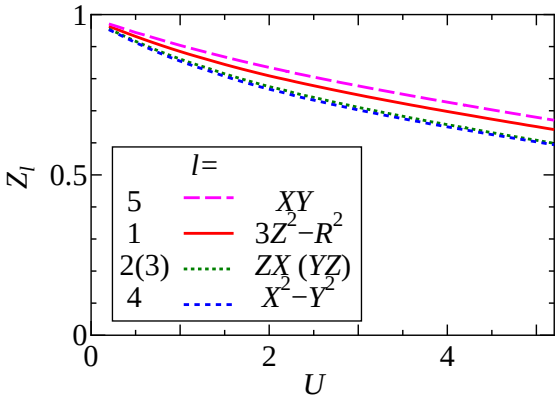

Fig. 2. (Color online) The renormalization factor Z_ℓ with $\ell = d_{3Z^2-R^2}, d_{ZX}, d_{YZ}, d_{X^2-Y^2}$, and d_{XY} as functions of U with $U = U' - 0.2$, $J = 0.15$ and $J = J'$ for $n = 6.0$ and $T = 0.02$.

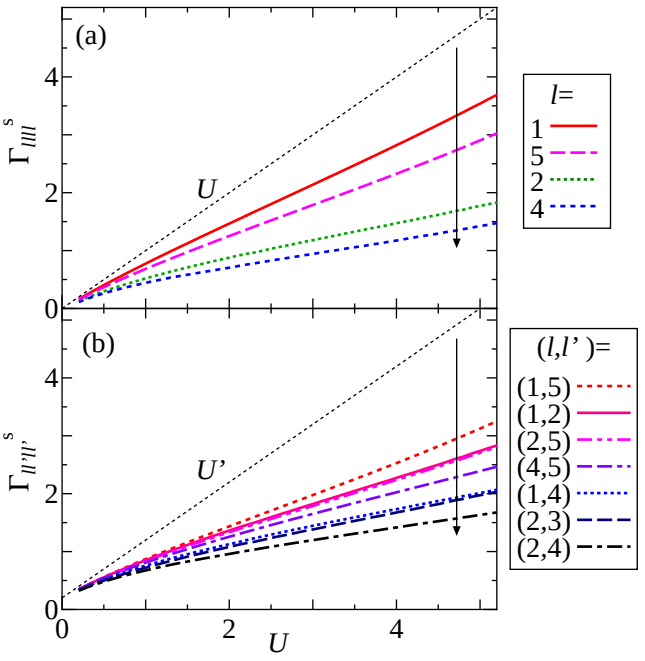

Fig. 3. (Color online) The spin vertex functions for the orbital-diagonal components $\Gamma^s_{\ell\ell\ell\ell}$ (a) and the orbital-off-diagonal components $\Gamma^s_{\ell\ell'\ell\ell'}$ (b) as functions of U. The bare vertices are also plotted by thin-dot lines.

3.1 Renormalization factor

First, we discuss the self-energy correction. Figure 2 shows the renormalization factor $Z_\ell = \left[1 - \frac{d\Sigma_\ell(\varepsilon)}{d(\varepsilon)}\Big|_{\varepsilon\to 0}\right]^{-1}$ for orbital ℓ as functions of U. Z_ℓ is almost independent of ℓ and gradually decreases with increasing U. As previously discussed by several authors,[39,43,44] the orbital dependence of Z_ℓ becomes large in the case with large J and/or U/U', where the magnetic fluctuation is dominated over the orbital one and the orbital selective Mott transition in which Z_ℓ with a specific ℓ exclusively becomes zero may occur. More generally, the imbalance between the magnetic and the orbital fluctuations is considered to be critical for enhancing the orbital dependence of Z_ℓ. Actually, the exclusively small Z_ℓ with $\ell = X^2 - Y^2$ was found for the both sides of the magnetic fluctuation-dominated case with $U > U'$ and the orbital fluctuation-dominated case with $U < U'$.[30] This is a striking contrast to the present case with $U \sim U'$ where the magnetic and the orbital fluctuations compete with each other resulting in the almost orbital-independent Z_ℓ as shown in Fig. 2.

3.2 Vertex function

Next, we discuss the spin and charge-orbital irreducible vertex functions with the lowest Matsubara frequency $i\omega_n = 0$, $\Gamma^{s(c)}_{\ell_1\ell_2\ell_3\ell_4} \equiv \hat{\Gamma}_{s(c)}(i\omega_n = 0)]_{\ell_1\ell_2\ell_3\ell_4}$, where the orbital-diagonal components $\Gamma^s_{\ell\ell\ell\ell}$ and the orbital-off-diagonal components $\Gamma^s_{\ell\ell'\ell\ell'}$ ($\ell \neq \ell'$) are compared with the corresponding non-zero components of the bare vertices $[\hat{\Gamma}^{(0)}_{s(c)}]_{\ell\ell\ell\ell}$ and $[\hat{\Gamma}^{(0)}_{s(c)}]_{\ell\ell'\ell\ell'}$ defined in the text below eq.(5).

Figures 3 (a) and (b) show the spin vertex functions $\Gamma^s_{\ell\ell\ell\ell}$ and $\Gamma^s_{\ell\ell'\ell\ell'}$ for various ℓ and $\ell'(\neq \ell)$ together with the corresponding bare vertices $[\hat{\Gamma}^{(0)}_s]_{\ell\ell\ell\ell} = U$ and $[\hat{\Gamma}^{(0)}_s]_{\ell\ell'\ell\ell'} = U'$, respectively. We find that $\hat{\Gamma}_s$ is strongly renormalized as U increases due to the correlation effect and shows the significant orbital dependence. As shown in Fig. 3 (a), the orbital-diagonal components $\Gamma^s_{\ell\ell\ell\ell}$ for $\ell = X^2 - Y^2, ZX/YZ$ are largely reduced while those for $\ell = XY, 3Z^2 - R^2$ are less reduced. This is considered due to the difference in the weights of each d orbital at the FSs: those are large for $\ell = X^2-Y^2, ZX/YZ$ while small for $\ell = XY, 3Z^2-R^2$, as shown in Figs. 1 (c)-(f). The strong reduction of the spin vertex for $\ell = X^2 - Y^2, ZX/YZ$ with the large orbital weights at the FSs may result in the suppression of the magnetic order due to the correlation effect which will be discussed in the next subsection.

In contrast to the spin vertex, the orbital-diagonal components of the charge vertex $\Gamma^c_{\ell\ell\ell\ell}$ becomes larger than the corresponding bare vertex $[\hat{\Gamma}^{(0)}_c]_{\ell\ell\ell\ell} = U$ as shown in Fig. 4 (a), resulting in the suppression of the charge susceptibility due to the correlation effect. On the other hands, the orbital-off-diagonal components of the charge vertex $\Gamma^c_{\ell\ell'\ell\ell'}$ are reduced as shown in Fig. 4 (b), resulting in the suppression of the orbital order due to the correlation effect which is similar to that of the magnetic order but is relatively smaller than the latter as explicitly shown in the next subsection.

The opposite renormalization effects between the spin and the charge vertices were previously discussed in the single-orbital Hubbard model on the basis of the DMFT[45] and the self-consistent fluctuation theory[46] with including the correlation effects beyond the RPA, where ones found that $\Gamma_s < \Gamma^{(0)} < \Gamma_c$ resulting in the suppression of both the spin and the charge susceptibilities as consistent with the present results for the orbital-diagonal components of the spin and the charge-orbital vertices. The orbital-off-diagonal components as well as the orbital dependence of the vertices, however, could not considered in the single-orbital model and are firstly discussed in the present paper. We note that the large orbital dependence of the vertex [see Figs. 3 and 4] together with the small orbital dependence of the renormalization factor [see Fig. 2] is a specific feature of the present case with $U \sim U'$ where the AFM and the AFO fluctuations are comparably enhanced. This is a striking contrast to the case with $U > U'$ ($U < U'$) where the AFM (AFO) fluctuation dominates over the AFO (AFM) one and the small orbital dependence of the vertex together with the large orbital dependence of the renor-

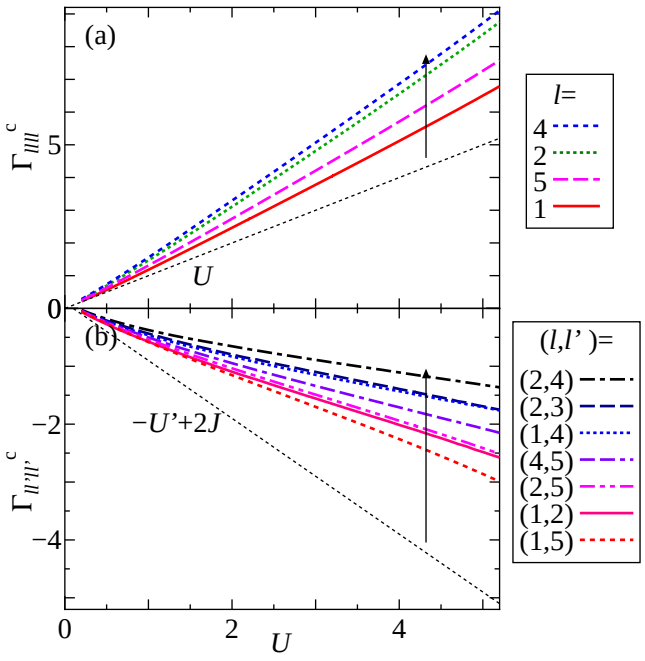

Fig. 4. (Color online) The charge-orbital vertex functions for the orbital-diagonal components $\Gamma^c_{\ell\ell\ell\ell}$ (a) and the orbital-off-diagonal components $\Gamma^c_{\ell\ell'\ell\ell'}$ (b) as functions of U. The bare vertices are also plotted by thin-dot lines.

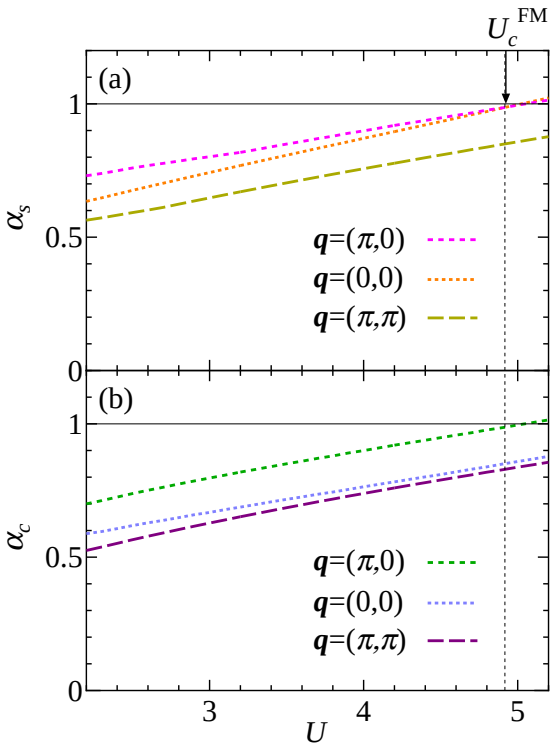

Fig. 5. (Color online) U-dependence of the spin and the charge-orbital Stoner factors $\alpha_s(\boldsymbol{q})$ (a) and $\alpha_c(\boldsymbol{q})$ (b) for several $\boldsymbol{q}$, which reach unity towards the magnetic and the charge-orbital instabilities. $U_c^{\rm FM}$ is the critical value towards the FM instability and is slightly smaller than the critical values towards the AFM and AFO instabilities.

malization factor responsible for the orbital selective Mott transition in the strong correlation regime is observed.[30)]

3.3 Spin and charge-orbital Stoner factors

Figures. 5 (a) and (b) show the U-dependence of the spin and the charge-orbital Stoner factors $\alpha_s(\boldsymbol{q})$ and $\alpha_c(\boldsymbol{q})$, respectively, for the wave vectors $\boldsymbol{q} = (\pi, 0)$, $(0, 0)$ and (π, π). The critical value towards the magnetic instability is found to be $U_c \sim 4.9$ and is largely suppressed as compared with the RPA result $U_c^{\rm RPA} \sim 0.8$ due to the self-energy and the vertex corrections within the DMFT. For small U, the stripe-type AFM and AFO fluctuations with $\boldsymbol{q} = (\pi, 0)$ are dominant over the other fluctuations. However, when U increases, the FM fluctuation with $\boldsymbol{q} = (0, 0)$ becomes competitive with the AFM and AFO fluctuations, and finally overcomes just below U_c where the FM instability takes place. The FM fluctuation originates from the $\boldsymbol{q} \sim (0, 0)$ nesting between the inner-hole FS1 with the large ZX/YZ orbital weights [see Fig.1 (c)] and the outer-hole FS2 with the large XY orbital weight [see Fig.1 (d)], and is enhanced by the inter-orbital Coulomb interaction between ZX/YZ and XY orbitals. This enhancement becomes significant for large U as the renormalization of the $d_{ZX/YZ}$-d_{XY} orbital-off-diagonal spin vertex is relatively smaller than that of the $d_{X^2-Y^2}$ and $d_{ZX/YZ}$ orbital-diagonal spin (charge-orbital) vertices [see Figs. 3 and 4] which enhance the AFM (AFO) fluctuation as shown in the next subsection.

To clarify the effects of the vertex corrections on the magnetic and the orbital fluctuations more explicitly, we estimate the spin and charge-orbital Stoner factors with the use of the approximate vertex in stead of the full DMFT vertex $\hat{\Gamma}_{s(c)}$ in eq. (3) as follows (see Table I): (i) When we approximately use the bare vertex $\hat{\Gamma}_{s(c)} \approx \hat{\Gamma}^{(0)}_{s(c)}$, the AFM fluctuation is exclusively enhanced similar to the case with the RPA. (ii) When we average over the orbital as $\hat{\Gamma}_{s(c)} \approx \langle\hat{\Gamma}_{s(c)}\rangle$, the AFO fluctuation is enhanced comparably to the AFM one due to the different renormalization between the spin and the charge-orbital vertices, but the enhancement of the FM fluctuation is relatively small as the orbital dependence of the spin vertex which is crucial for the FM fluctuation enhancement as mentioned above is neglected. (iii) When we use the full DMFT vertices $\hat{\Gamma}_{s(c)}$, the AFM, FM and AFO fluctuations are comparably enhanced due to the orbital dependence of the vertices together with the different renormalization between the spin and the charge-orbital vertices.

	vertex	$\alpha_s^{\rm AFM}$	$\alpha_s^{\rm FM}$	$\alpha_c^{\rm AFO}$	$\alpha_c^{\rm FO}$
(i)	bare	1.000	0.498	0.727	0.586
(ii)	orbital-averaged	1.000	0.766	0.966	0.785
(iii)	full DMFT	1.000	1.003	1.001	0.863

Table I. Spin and charge-orbital Stoner factors $\alpha_s(\boldsymbol{q})$ and $\alpha_c(\boldsymbol{q})$ for $\boldsymbol{q} = (\pi, 0)$ and $\boldsymbol{q} = (0, 0)$, in the cases with (i) the bare vertex $\hat{\Gamma}_{s(c)} \approx \hat{\Gamma}^{(0)}_{s(c)}$, (ii) the orbital-averaged vertex $\hat{\Gamma}_{s(c)} \approx \langle\hat{\Gamma}_{s(c)}\rangle$ and (iii) the full DMFT vertex $\hat{\Gamma}_{s(c)}$, where we set (i) $U = 0.76$, (ii) $U = 2.66$ and (iii) $U = 5.05$ so as to fix $\alpha_s^{\rm AFM} = 1$ for all cases.

3.4 Susceptibility and effective pairing interaction

Figures 6 (a) and (b) show the orbital-diagonal and the orbital-off-diagonal components of the spin susceptibility $\chi^s_{\ell,\ell;m,m}$ and $\chi^s_{\ell,m;\ell,m}$ as functions of the wave vector $\boldsymbol{q}$ with

the lowest Matsubara frequency $i\omega_n = 0$ for $U = 4.5$ where the spin Stoner factor is $\alpha_s = 0.958$. The $d_{X^2-Y^2}$ intra-orbital spin susceptibility $\chi^s_{4,4;4,4}$ is largely enhanced around $\boldsymbol{q} \sim (\pi, 0)$ [see Fig. 6 (a)] due to the effect of the intra-orbital nesting between the hole FS3 and the electron FS, where the weights of the $d_{X^2-Y^2}$ component are large in the both FSs as shown in Fig. 1 (e) and (f). Then, the $d_{X^2-Y^2}$ orbital is mainly responsible for the spin susceptibility $\sum_{\ell,m} \chi^s_{\ell,\ell;m,m}$ around $\boldsymbol{q} \sim (\pi, 0)$. Note that the inter-orbital spin susceptibility $\chi^s_{2,4;2,4}$ is also enhanced for $\boldsymbol{q} \sim (\pi, 0)$ [see Fig. 6 (b)] due to the effect of the inter-orbital ($d_{ZX/YZ}$-$d_{X^2-Y^2}$) nesting between the hole FS2 and the electron FS.

In addition to the intra- and inter-orbital spin susceptibilities with $\boldsymbol{q} \sim (\pi, 0)$, the inter-orbital spin susceptibility $\chi^s_{2,5;2,5}$ around $\boldsymbol{q} \sim (0, 0)$ is largely enhanced due to the inter-orbital ($d_{ZX/YZ}$-d_{XY}) nesting between the inner (FS1) and the outer (FS2) hole FSs as shown in Fig.6 (b). As mentioned before, the orbital-dependent spin vertex with relatively large value of the $d_{ZX/YZ}$-d_{XY} orbital-off-diagonal component is crucial for the FM fluctuation enhancement, that is a remarkable correlation effect beyond the RPA.

Figure 6 (c) shows the several components of the charge-orbital susceptibility as functions of $\boldsymbol{q}$ with the lowest Matsubara frequency $i\omega_n = 0$ for $U = 4.5$, where the charge-orbital Stoner factor is $\alpha_c = 0.958$. Similar to the spin susceptibility, both the intra- and inter-orbital charge-orbital susceptibilities are largely enhanced around $\boldsymbol{q} \sim (\pi, 0)$ due to the intra- and inter-orbital nesting effects. In the present case, one observes $\chi^c_{4,4;4,4} \approx \chi^c_{2,4;2,4}$ for $\boldsymbol{q} \sim (\pi, 0)$.

In Fig. 6 (d), the several components of the effective pairing interaction $\hat{V}(q)$ are plotted as functions of $\boldsymbol{q}$ with the lowest Matsubara frequency $i\omega_n = 0$ for $U = 4.5$. The inter-orbital component $V_{2,5;2,5}$ becomes very large around $\boldsymbol{q} \sim (0, 0)$ due to the inter-orbital FM fluctuation [see Fig.6 (b)]. Various components of $\hat{V}(q)$ show peaks at $\boldsymbol{q} \sim (\pi, 0)$, where the AFM fluctuation-mediated repulsive pairing interaction is partially canceled by the AFO fluctuation-mediated attractive one as seen from the 1st. and 2nd. terms of r.h.s. in eq. (5), resulting in the moderate peak of $\hat{V}(q)$ at $\boldsymbol{q} \sim (\pi, 0)$ in contrast to the large peak at $\boldsymbol{q} \sim (0, 0)$ where the FO fluctuation is not so enhanced [see Fig. 6 (c)] and such cancellation effect is small.

3.5 *Superconducting gap function*

Finally, we discuss the superconductivity when the FM, AFM and AFO fluctuations are comparably enhanced. In Figures 7 (a)-(c), we show the gap functions $\Delta_s(\boldsymbol{k})$ in the band representation for the band $s = 2 - 4$ with the lowest Matsubara frequency $i\varepsilon_m = i\pi T$ for $U = 4.5$. We observe a specific hole-$s_{\pm}$-wave pairing, where the gap function changes its sign between the inner-hole FS1 and the outer-hole FS2 due to the large repulsive pairing interaction $V_{2,5;2,5}$ around $\boldsymbol{q} \sim (0, 0)$ mediated by the FM fluctuation, and also changes between the inner-hole FS1 and the electron FS due to the moderate repulsive pairing interaction around $\boldsymbol{q} \sim (\pi, 0)$ mediated by the AFM fluctuation [see Fig. 6 (d)]. It is noted that we also observe the sign change of the gap function in the orbital representation between the ZX/YZ and the XY orbitals (not shown). The obtained hole-$s_{\pm}$-wave state has the same sign between the hole FS2, FS3 and the electron FS and the sign of the gap function of each FS is summarized as $(\Delta_{h1}, \Delta_{h2}, \Delta_{h3}, \Delta_e) = (-, +, +, +)$ which is different from the pairing states previously proposed for LiFeAs with $(\Delta_{h1}, \Delta_{h2}, \Delta_{h3}, \Delta_e) = (+, +, -, +)$, $(-, +, -, +)$, $(+, +, -, -)$,[27–29] where the correlation induced FM fluctuation which is crucial for the present result is not taken into account.

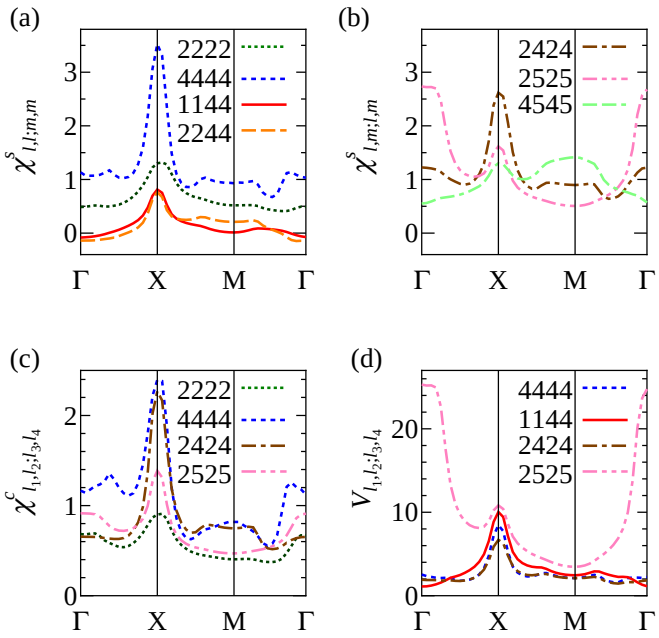

Fig. 6. (Color online) The orbital-diagonal and the orbital-off-diagonal components of the spin susceptibility $\chi^s_{\ell,\ell;m,m}$ (a) and $\chi^s_{\ell,m;\ell,m}$ (b), the several components of the charge-orbital susceptibility $\hat{\chi}^c$ (c) and the several components of the pairing interaction $\hat{V}$ (d) as functions of $\boldsymbol{q}$ with the lowest Matsubara frequency $i\omega_n = 0$ for $U = 4.5$, where $\alpha_s = 0.958$ and $\alpha_c = 0.958$.

In general, the FM fluctuation is considered to mediate the spin-triplet pairing. As for the iron-pnictides, Brydon *et al.* discussed the spin-triplet p-wave pairing mediated by the nearly FM fluctuation within the RPA for the three-orbital Hubbard model.[26] Then, let us discuss the possibility of the spin-triplet pairing in the present model eq (1) on the basis of the DMFT combined with the Eliashberg equation, where the effective pairing interaction for the spin-triplet state:

$$\hat{V}(q) = -\frac{1}{2}\hat{\Gamma}_s(i\omega_n)\hat{\chi}_s(q)\hat{\Gamma}_s(i\omega_n) - \frac{1}{2}\hat{\Gamma}_c(i\omega_n)\hat{\chi}_c(q)\hat{\Gamma}_c(i\omega_n) + \frac{1}{2}\left(\hat{\Gamma}^{(0)}_s + \hat{\Gamma}^{(0)}_c\right), \quad (7)$$

is substituted into eq. (6) instead of that for the spin-singlet state given in eq, (5). Here, we consider only the p_x-wave state, because the present model is symmetric under rotation in spin space and then all p-wave states are degenerate in principle. The largest eigenvalues of the Eliashberg equation λ for the singlet and the triplet states are plotted in Fig. 8. When U increases, λ for the triplet state increases with increasing the FM fluctuation as expected, but is always smaller than λ for the singlet state, that is a specific feature of the present multi-orbital model in the case with competing FM, AFM and AFO fluctuations. Thus, we conclude that the expected pairing state is the spin-singlet hole-$s_{\pm}$-wave.

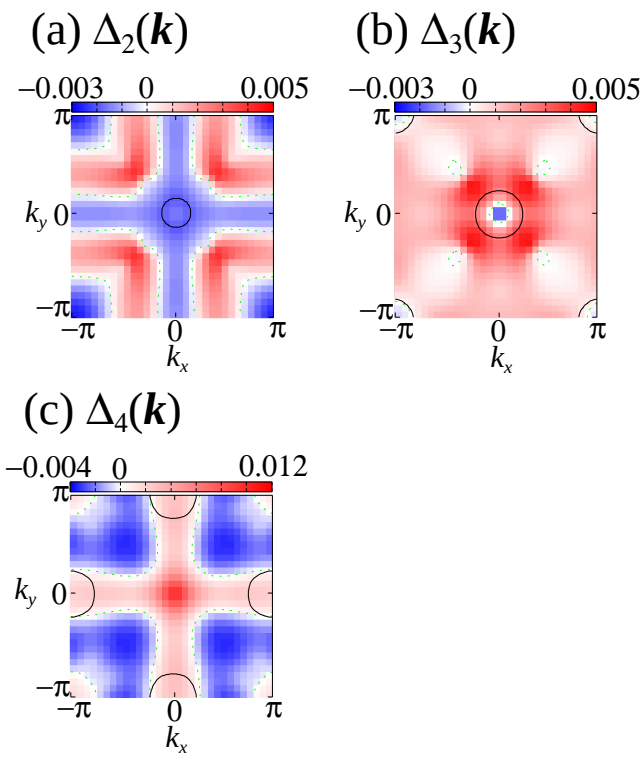

Fig. 7. (Color online) The band representation of the superconducting gap functions $\Delta_s(\boldsymbol{k})$ on the $\boldsymbol{k}$-plane for the band $s = 2-4$ with the lowest Matsubara frequency $i\varepsilon_m = i\pi T$ for $U = 4.5$, where the largest eigenvalue of the Eliashberg equation is $\lambda = 1.07$, together with the FSs (solid lines): hole FS1 in (a), hole FS2 and FS3 in (b) and electron FS in (c).

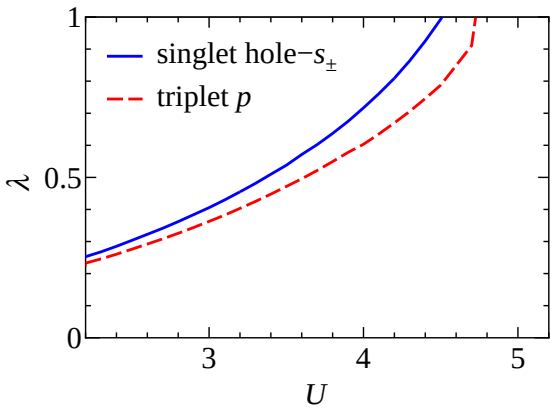

Fig. 8. (Color online) The largest eigenvalues of the Eliashberg equation λ for the spin-singlet and the spin-triplet states as functions of U.

4. Summary and discussion

In summary, we have investigated the electronic states and the superconductivity in the five-orbital Hubbard model for iron-based superconductors by using the DMFT combined with the Eliashberg equation to clarify the strong correlation effects, especially focusing on the specific case with U being a little smaller than U' where the AFM and the AFO fluctuations are comparably enhanced. When U increases, the renormalization factor Z_l obtained from the self-energy monotonically decreases almost independent of the orbital l even for large U in contrast to the previously discussed case with $U > U'$ ($U < U'$) where the AFM (AFO) fluctuation dominates over the AFO (AFM) one and the large l-dependence of Z_l responsible for the orbital selective Mott transition for large U is observed.[30] On the other hand, the l-dependence of the spin and charge-orbital vertices is large in contrast to the previous case where that is small.[30] The renormalization of the $d_{ZX/YZ}$-d_{XY} orbital-off-diagonal spin vertex responsible for the FM fluctuation enhancement is relatively smaller than that of the $d_{X^2-Y^2}$ and $d_{ZX/YZ}$ orbital-diagonal spin (charge-orbital) vertices responsible for the AFM (AFO) fluctuation enhancement. Therefore, the FM fluctuation is enhanced larger than the AFM and AFO ones and finally overcomes those for large U, where the FM instability takes place at U_c just below the AFM and AFO instabilities. In this case, the effective pairing interaction $\hat{V}(q)$ shows a large peak at $\boldsymbol{q} \sim (0,0)$ while a small one at $\boldsymbol{q} \sim (\pi,0)$ where the effects of the AFM and AFO fluctuations are compete with each other, resulting in the remarkable hole-$s_\pm$-wave pairing with the sign change of the gap function between the inner and outer hole FSs.

Previously, several authors[27–29] proposed the orbital antiphase $s_\pm$-wave and the hole-$s_\pm$-wave symmetries as promising pairing states for LiFeAs, but the relative signs of the gap function on the FSs are different from the present result. The most significant difference between the previous and the present hole-$s_\pm$-wave states is the pairing mechanism: the most dominant pairing interaction in the present theory is between the inner and outer hole FSs at $\boldsymbol{q} \sim (0,0)$ mediated by the largely enhanced FM fluctuation which was not taken into account in the previous theories but was observed by the μSR experiment.[23] The nodeless gap structure in LiFeAs observed by the ARPES experiment[33] seems to be consistent with the hole-$s_\pm$-wave states as well as the other s-wave states such as the $s_\pm$- and the s_{++}-wave states, but it is difficult to distinguish between the various s-wave states at the moment because of the difficulty to determine the relative sign of the gap function on the different FSs.[47–49]

The enhanced FM fluctuation was previously obtained in the three-orbital Hubbard model for LiFeAs, where the flatness of the hole band top yields the large density of states near the Fermi level responsible for the Stoner enhancement of the magnetic susceptibility within the RPA, and was considered to mediate the spin-triplet p-wave pairing with nodes of the gap function on the hole band.[26] This is a striking contrast to the present theory where the strong correlation effect is crucial for enhancing the orbital-off-diagonal FM fluctuation which mediates the spin-singlet hole-$s_\pm$-wave pairing without nodes as consistent with the ARPES experiment[33] mentioned above. In addition, the NMR measurements for LiFeAs,[50–52] where the Knight shift decreases with decreasing T below T_c, also seems to be consistent with the spin-singlet pairing.

Finally, we make a brief discussion on the frequency dependence of the vertex functions including the retardation effect of the pairing interaction which is known to enhance the superconducting transition temperature.[53,54] Although the frequency dependence of the vertex functions was neglected to solve the linearized Eliashberg equation in this paper, we have also made some preliminary calculations with the frequency dependent vertex functions which are largely renormalized as $\hat{\Gamma}_{s(c)}(i\omega_n) \sim \hat{\Gamma}_{s(c)}(0)$ for small ω_m while are approximately

given by the bare vertices as $\hat{\Gamma}_{s(c)}(i\omega_n) \sim \hat{\Gamma}^{(0)}_{s(c)}$ for large ω_m, and have found that the obtained λ is actually enhanced as compared with the results without the frequency dependence. To be more conclusive, we need to obtain the precise vertex functions depending on not only the external frequency but also the internal ones which were not taken into account in the present paper but is considered to play important roles especially in the strong correlation regime and will be explicitly discussed in a subsequent paper.

Acknowledgments

This work was partially supported by a Grant-in-Aid for Scientific Research from the Ministry of Education, Culture, Sports, Science and Technology.

1) Y. Kamihara, H. Hiramatsu, M. Hirano, R. Kawamura, H. Yanagi, T. Kamiya, and H. Hosono: J. Am. Chem. Soc. **128** (2006) 10012.
2) D. C. Johnston: Adv. Phys **59** (2010) 803.
3) P. J. Hirschfeld, M. M. Korshunov, and I. I. Mazin: Rep. Prog. Phys **74** (2011) 124508.
4) R. M. Fernandes, L. H. VanBebber, S. Bhattacharya, P. Chandra, V. Keppens, D. Mandrus, M. A. McGuire, B. C. Sales, A. S. Sefat, and J. Schmalian: Phys. Rev. Lett **105** (2010) 157003.
5) T. Goto, R. Kurihara, K. Araki, K. Mitsumoto, M. Akatsu, Y. Nemoto, S. Tatematsu, and M. Sato: J. Phys. Soc. Jpn **80** (2011) 073702.
6) M. Yoshizawa, D. Kimura, T. Chiba, A. Simayil, Y. Nakanishi, K. Kihou, C.-H. Lee, A. Iyo, H. Eisaki, M. Nakajima, and S. Uchida: J. Phys. Soc. Jpn **81** (2012) 024604.
7) I. I. Mazin, D. J. Singh, M. D. Johannes, and M. H. Du: Phys. Rev. Lett **101** (2008) 057003.
8) K. Kuroki, S. Onari, R. Arita, H. Usui, Y. Tanaka, H. Kontani, and H. Aoki: Phys. Rev. Lett **101** (2008) 087004.
9) Y. Yanagi, Y. Yamakawa, N. Adachi, and Y. Ōno: J. Phys. Soc. Jpn **79** (2010) 123707.
10) H. Kontani, T. Saito, and S. Onari: Phys. Rev. B **84** (2011) 024528.
11) S. Onari and H. Kontani: Phys. Rev. Lett **109** (2012) 137001.
12) H. Kontani and S. Onari: Phys. Rev. Lett **104** (2010) 157001.
13) Y. Yanagi, Y. Yamakawa, N. Adachi, and Y. Ōno: Phys. Rev. B **82** (2010) 064518.
14) The frequency $\omega(\boldsymbol{q})$ of a phonon coupled to a quadrupole O is renormalized as $\omega(\boldsymbol{q})/\omega^0(\boldsymbol{q}) = [\chi^{\rm irr}_O(\boldsymbol{q},0)/\chi_O(\boldsymbol{q},0)]^{1/2}$ and is expected to show a softening for $\boldsymbol{q} \sim \boldsymbol{Q}_{\rm AF}$ due to the enhancement of the AFO fluctuation as observed for the acoustic phonon softened for $\boldsymbol{q} \sim \boldsymbol{0}$ due to the FO fluctuation.
15) T. Yamada, J. Ishizuka, and Y. Ōno: J. Phys. Soc. Jpn **83** (2014) 043704.
16) C. Ma, L. Wu, W. Yin, H. Yang, H. Si, Z. Wang, J. Li, C. Homes, and Y. Zhu: Phys. Rev. Lett **112** (2014) 077001.
17) T. Miyake, K. Nakamura, R. Arita, and M. Imada: J. Phys. Soc. Jpn. **79** (2010) 0447105.
18) J. Ishizuka, T. Yamada, Y. Yanagi, and Y. Ōno: preprint .
19) J. H. Tapp, Z. Tang, B. Lv, K. Sasmal, B. Lorenz, P. C. W. Chu, and A. M. Guloy: Phys. Rev. B **78** (2008) 060505(R).
20) A. E. Taylor, M. J. Pitcher, R. A. Ewings, T. G. Perring, S. J. Clarke, and A. T. Boothroyd: Phys. Rev. B **83** (2011) 220514(R).
21) N. Qureshi, Y. Drees, J. Werner, S. Wurmehl, C. Hess, R. Klingeler, B. Buchner, M. T. Fernandez-Diaz, and M. Braden: Phys. Rev. B **82** (2010) 184521.
22) J. Knolle, V. B. Zabolotnyy, I. Eremin, S. V. Borisenko, N. Qureshi, M. Braden, D. V. Evtushinsky, T. K. Kim, A. A. Kordyuk, S. Sykora, C. Hess, I. V. Morozov, S. Wurmehl, R. Moessner, and B. Büchner: Phys. Rev. B **86** (2012) 174519.
23) J. D. Wright, M. J. Pitcher, W. Trevelyan-Thomas, T. Lancaster, P. J. Baker, F. L. Pratt, S. J. Clarke, and S. J. Blundell: Phys. Rev. B **88** (2013) 060401.
24) P. Wiecki, B. Roy, D. C. Johnston, S. L. Bud'ko, P. C. Canfield, and Y. Furukawa: Phys. Rev. Lett. **115** (2015) 137001.
25) I. I. Mazin, D. J. Singh, M. D. Johannes, and M. H. Du: Phys. Rev. Lett. **101** (2008) 057003.
26) P. M. R. Brydon, M. Daghofer, C. Timm, and J. van den Brink: Phys. Rev. B **83** (2011) 060501.
27) Z. P. Yin, K. Haule, and G. Kotliar: Nat Phys. **10** (2014) 845.
28) F. Ahn, I. Eremin, J. Knolle, V. B. Zabolotnyy, S. V. Borisenko, B. Büchner, and A. V. Chubukov: Phys. Rev. B **89** (2014) 144513.
29) T. Saito, S. Onari, Y. Yamakawa, H. Kontani, S. V. Borisenko, and V. B. Zabolotnyy: Phys. Rev. B **90** (2014) 035104.
30) J. Ishizuka, T. Yamada, Y. Yanagi, and Y. Ōno: J. Phys. Soc. Jpn. **82** (2013) 123712.
31) H. Kontani and S. Onari: Phys. Rev. Lett. **104** (2010) 157001.
32) Y. Yanagi, Y. Yamakawa, N. Adachi, and Y. Ōno: Phys. Rev. B **82** (2010) 064518.
33) S. V. Borisenko, V. B. Zabolotnyy, A. A. Kordyuk, D. V. Evtushinsky, T. K. Kim, I. V. Morozov, R. Follath, and B. Büchner: Symmetry **4** (2012) 251.
34) K. Kuroki, S. Onari, R. Arita, H. Usui, Y. Tanaka, H. Kontani, and H. Aoki: Phys. Rev. Lett. **101** (2008) 087004.
35) A. Georges, G. Kotliar, W. Krauth, and M. J. Rozenberg: Rev. Mod. Phys **68** (1996) 13.
36) J. Ishizuka, T. Yamada, Y. Yanagi, and Y. Ōno: JPS Conf. Proc. **3** (2014) 015020.
37) M. Yi, D. H. Lu, R. Yu, S. C. Riggs, J.-H. Chu, B. Lv, Z. K. Liu, M. Lu, Y.-T. Cui, M. Hashimoto, S.-K. Mo, Z. Hussain, C. W. Chu, I. R. Fisher, Q. Si, and Z.-X. Shen: Phys. Rev. Lett. **110** (2013) 067003.
38) L. de' Medici, S. R. Hassan, and M. Capone: J. Supercond. Nov. Magn. **22** (2009) 535.
39) L. de' Medici, S. R. Hassan, M. Capone, and X. Dai: Phys. Rev. Lett. **102** (2009) 126401.
40) F. Hard, A. E. Bohmer, D. Aoki, P. Burge, T. Wolf, P. Schweiss, R. Heid, P. Adelmann, Y. X. Yao, G. Kotliar, J. Schmalian, and C. Meingast: Phys. Rev. Lett. **111** (2013) 027002.
41) M. Aichhorn, L. Pourovskii, and A. Georges: Phys. Rev. B **84** (2011) 054529.
42) H. Park, K. Haule, and G. Kotliar: Phys. Rev. Lett. **107** (2011) 137007.
43) A. Koga, N. Kawakami, T. M. Rice, and M. Sigrist: Phys. Rev. B **72** (2005) 045128.
44) M. Ferrero, F. Becca, M. Fabrizio, and M. Capone: Phys. Rev. B **72** (2005) 205126.
45) G. Rohringer, A. Valli, and A. Toschi: Phys. Rev. B **86** (2012) 125114.
46) H. Kusunose: J. Phys. Soc. Jpn. **79** (2010) 094707.
47) T. Hänke, S. Sykora, R. Schlegel, D. Baumann, L. Harnagea, S. Wurmehl, M. Daghofer, B. Büchner, J. van den Brink, and C. Hess: Phys. Rev. Lett. **108** (2012) 127001.
48) M. P. Allan, A. W. Rost, A. P. Mackenzie, Y. Xie, J. C. Davis, K. Kihou, C. H. Lee, A. Iyo, H. Eisaki, and T.-M. Chuang: Science **336** (2012) 563.
49) C. Hess, S. Sykora, T. Hänke, R. Schlegel, D. Baumann, V. B. Zabolotnyy, L. Harnagea, S. Wurmehl, J. van den Brink, and B. Büchner: Phys. Rev. Lett. **110** (2013) 017006.
50) Z. Li, Y. Ooe, X.-C. Wang, Q.-Q. Liu, C.-Q. Jin, M. Ichioka, and G. qing Zheng: J. Phys. Soc. Jpn. **79** (2010) 083702.
51) P. Jeglič, A. Potočnik, M. Klanjšek, M. Bobnar, M. Jagodič, K. Koch, H. Rosner, S. Margadonna, B. Lv, A. M. Guloy, and D. Arčon: Phys. Rev. B **81** (2010) 140511.
52) S.-H. Baek, L. Harnagea, S. Wurmehl, B. Büchner, and H.-J. Grafe: J. Phys.: Condens. Matter **25** (2013) 162204.
53) P. Morel and P. W. Anderson: Phys. Rev. **125** (1962) 1263.
54) Y. Takada: J. Phys. Soc. Jpn. **78** (2009) 013703.